Evolution of *E. coli* in a mouse model of inflammatory bowel disease leads to a disease-specific bacterial genotype and trade-offs with clinical relevance

Rahul Unni[1,2,#], Nadia Andrea Andreani[1,2,#], Marie Vallier[1,2,§,#], Silke S. Heinzmann[3], Jan Taubenheim[4], Martina A. Guggeis[5,6], Florian Tran[5,6], Olga Vogler[1], Sven Künzel[1], Jan-Bernd Hövener[7], Philip Rosenstiel[5], Christoph Kaleta[4], Astrid Dempfle[8], Daniel Unterweger[1,2,*], John F. Baines[1,2,*]

[1] *Max Planck Institute for Evolutionary Biology, Plön, Germany.*

[2] *Section of Evolutionary Medicine, Institute for Experimental Medicine, Kiel University, Kiel, Germany.*

[3] *Research Unit Analytical BioGeoChemistry, Helmholtz Munich, Neuherberg, Germany.*

[4] *Research Group Medical Systems Biology, Institute for Experimental Medicine, Kiel University, Kiel, Germany.*

[5] *Institute of Clinical Molecular Biology, Christian-Albrechts-University Kiel and University Medical Center Schleswig-Holstein, Kiel, Germany.*

[6] *Department of Internal Medicine I, University Medical Center Schleswig-Holstein, Kiel, Germany.*

[7] *Section Biomedical Imaging, Molecular Imaging North Competence Center (MOIN CC), Department of Radiology and Neuroradiology, University Medical Center Kiel, Kiel University, Kiel, Germany.*

[8] *Institute of Medical Informatics and Statistics, Kiel University, Kiel, Germany.*

[#] These authors contributed equally.

[§] Current affiliation: Valbiotis, R&D Center, Riom, France.

* Corresponding authors: baines@evolbio.mpg.de, unterweger@iem.uni-kiel.de

ORCID:

Rahul Unni: 0000-0002-4656-7542

Nadia Andrea Andreani: 0000-0003-0330-9874

Marie Vallier: 0000-0002-7188-7070

Silke Heinzmann: 0000-0003-0257-8837

Jan Taubenheim: 0000-0001-7283-1768

Martina A. Guggeis: 0000-0003-4505-3731

Florian Tran: 0000-0002-3735-9872

Olga Vogler: 0000-0001-8930-7671

Sven Künzel:

Jan-Bernd Hövener: 0000-0001-7255-7252

Philip Rosenstiel: 0000-0002-9692-8828

Christoph Kaleta: 0000-0001-8004-9514

Astrid Dempfle: 0000-0002-2618-3920

Daniel Unterweger: 0000-0001-7459-6386

John F. Baines: 0000-0002-8132-4909

Evolution of *E. coli* in a mouse model of inflammatory bowel disease leads to a disease-specific bacterial genotype and trade-offs with clinical relevance

Abstract

Inflammatory bowel disease (IBD) is a persistent inflammatory condition that affects the gastrointestinal tract and presents significant challenges in its management and treatment. Despite the knowledge that within-host bacterial evolution occurs in the intestine, the disease has rarely been studied from an evolutionary perspective. In this study, we aimed to investigate the evolution of resident bacteria during intestinal inflammation and whether- and how disease-related bacterial genetic changes may present trade-offs with potential therapeutic importance. Here, we perform an *in vivo* evolution experiment of *E. coli* in a gnotobiotic mouse model of IBD, followed by multiomic analyses to identify disease-specific genetic and phenotypic changes in bacteria that evolved in an inflamed versus a non-inflamed control environment. Our results demonstrate distinct evolutionary changes in *E. coli* specific to inflammation, including a single nucleotide variant that independently reached high frequency in all inflamed mice. Using *ex vivo* fitness assays, we find that these changes are associated with a higher fitness in an inflamed environment compared to isolates derived from non-inflamed mice. Further, using large-scale phenotypic assays, we show that bacterial adaptation to inflammation results in clinically relevant phenotypes, which intriguingly include collateral sensitivity to antibiotics. Bacterial evolution in an inflamed gut yields specific genetic and phenotypic signatures. These results may serve as a basis for developing novel evolution-informed treatment approaches for patients with intestinal inflammation.

Keywords: Inflammatory bowel disease, *E. coli*, experimental evolution, evolutionary trade-offs.

Introduction

Dysbiosis of the intestinal microbial community, characterized by alterations in bacterial composition and function, is a hallmark of inflammatory bowel disease (IBD). The nature of these microbial imbalances has been described extensively and at numerous complementary levels, including diversity parameters, taxonomic- and functional genomic changes, and at the level of gene expression [1–6]. This important body of work accounts for changes observed at the ecological level, while the latter also considers the potential contribution of phenotypic plasticity of gut microbes to disease susceptibility. Moreover, numerous studies have highlighted the association of dysbiotic microbial signatures with distinct clinical IBD subtypes, including Crohn's disease (CD) and ulcerative colitis (UC), further emphasizing the intricate relationship between the gut microbiota and disease pathogenesis [3,4,7].

While research has focused extensively on the altered ecology of the gut microbiota in IBD, its potential for evolutionary change during disease pathogenesis has received comparatively limited attention. However, numerous recent studies have revealed the capacity of bacteria to undergo adaptive evolution within the host environment, including the gut [reviewed in [8]]. This phenomenon is evident in both mouse models [9–11] and human subjects [12], even in the absence of overt disease. Importantly, recent studies indicate that evolutionary changes also occur in the context of host inflammation. Elhenawy et al. focused on CD-related adherent-invasive *E. coli* (AIEC) using a murine model of chronic colonization, and revealed the evolution of lineages displaying enhanced invasive and metabolic capabilities [13]. Notably, they found that the fitness benefits conferred by increased motility were specific to the host environment, suggesting an evolutionary trade-off. In a second study exploring bacterial evolution in aging mice, significant differences in *E. coli* evolution between old and young mice were revealed [14]. The aged mouse environment

97 exhibited increased inflammation, leading to the specific targeting of stress-related functions
98 in *E. coli*.

99 These findings emphasize the importance of including evolutionary perspectives
100 when studying dysbiosis of the gut microbiome. In particular, documenting bacterial
101 evolution within the inflamed gut has the potential to reveal the *timing* of disease-specific
102 signatures, i.e., it may help disentangle the classical "chicken or egg" dilemma in microbiome
103 research [15], as well as to shed light on potential trade-offs resulting from adaptive changes.
104 Evolutionary trade-offs occur when an increase in fitness in one environment is accompanied
105 by a decrease in fitness in another [16,17]. These trade-offs can have significant therapeutic
106 implications and are observed in various related fields, including antibiotic resistance [18–21]
107 and cancer treatment [22–25]. Thus, elucidating trade-offs associated with bacterial adaptations
108 in the inflamed gut may offer insight into potential collateral effects on bacterial fitness and
109 prove useful for developing novel treatment strategies based on evolutionary principles.

110 In this study, we investigated the evolutionary dynamics of resident gut bacteria
111 during intestinal inflammation using an established gnotobiotic mouse model of IBD [26].
112 Through the monocolonization of both *Interleukin 10*-knockout and wildtype mice with a
113 single *E. coli* strain (NC101), this setup allowed us to track genetic and phenotypic changes
114 over the course of intestinal inflammation and to evaluate their potential clinical relevance.
115 By employing multiomic analysis and high-throughput phenotypic screening, we identify
116 genetic changes in bacteria, alterations in the metabolome, and differences in numerous
117 phenotypic traits among bacterial populations that are specifically associated with the
118 evolution in inflamed *Il10*-knockout mice. Remarkably, among the phenotypic changes
119 observed in inflammation-adapted bacteria are sensitivities to antibiotics with a known
120 therapeutic value in IBD. These results further confirm the importance of understanding

121 bacterial adaptation to inflammation and suggest its more widespread study of patients as a
122 means to develop novel treatment approaches.

123 **Results**

124 ***Gnotobiotic model of intestinal inflammation***

125 In order to capture the evolutionary dynamics of bacteria evolving in the context of
126 intestinal inflammation, we implemented a previously established gnotobiotic model, for
127 which inflammation develops upon colonization with the *E. coli* NC101 strain in IL10-
128 deficient (*Il10*$^{-/-}$; herein "KO"), but not wild type (WT) mice [26]. We performed two
129 independent *in vivo* experiments (see Methods), in which WT (total N=14) and KO (total
130 N=11) mice were monocolonized and monitored over a period of 12 weeks, with longitudinal
131 sampling of feces for downstream multiomic analyses (Fig 1A; Table S1, see Methods).
132 Inflammation was monitored via levels of lipocalin-2 in feces, which steadily and
133 significantly increased in KO mice, but not in WT mice, already at one week post-inoculation
134 (Fig 1B, Tables S2 and S3, Wilcoxon signed-rank test Benjamini-Hochberg-corrected $P <$
135 0.05). Histopathological assessment of colonic tissue at the endpoint reveals significantly
136 higher pathology scores in KO mice than in WT mice (Fig 1C, Kruskal-Wallis H test
137 Benjamini-Hochberg-corrected $P < 0.05$), further confirming that inflammation was specific
138 to KO mice. The bacterial load in the fecal samples was stable throughout the experiment, as
139 measured by CFU counts normalized by wet feces weight (Fig S1, Tables S4 and S5).

140 ***Bacterial populations show genetic diversification in healthy and inflamed mice***

141 To assess the genetic diversification of the bacterial populations during the evolution
142 experiment, we performed shotgun sequencing on each single inoculum and all bacterial
143 populations at weeks 1, 4, 8, and 12 and identified *de-novo* mutations (i.e., mutations that

144 were not present in an inoculum; see Methods) by comparison with the genome of the
145 ancestral strain. No statistically significant difference was observed in the number of
146 mutations in the bacteria from KO and WT mice at any point in the experiment, suggesting
147 that differences in the intestinal environment in which the populations evolved did not exert a
148 measurable effect on the number of mutations (Fig S2, Table S6). One week after gavage, the
149 bacterial populations showed a median number of 87 *de-novo* mutations, with a subsequent
150 reduction at the following timepoints, although the differences are not significant (median at
151 week 4=34, at week 8=45 and at week 12=36, Fig S2, Tab S7 Wilcoxon signed rank test,
152 corrected $P > 0.05$). Comparison of the evolved populations at week 12 with the ancestral
153 strain reveals a median number of 39 mutations per mouse in WT and 26 in KO mice (Fig
154 1D). This indicates that the evolved bacterial populations in both groups of mice genetically
155 differ from the ancestral strain. Although the unphased shotgun data do not enable us to
156 directly analyze the role of genetic hitchhiking, Table S8 indicates the number of mutations at
157 week 12 already present at each earlier time point. Interestingly, there remains a substantial
158 (on average approx. 60% in each mouse genotype) proportion of *de-novo* mutations that arose
159 between week 8 and 12, which suggests that a large proportion of the mutations cannot be
160 explained by hitchhiking from standing genetic variation at earlier time points.

161 To test for overall differences in the *de-novo* mutations that accumulated in the
162 bacterial populations that evolved in the WT and KO mice, we performed a partial least-
163 squares discriminant analysis (PLS-DA) on all mutated loci (genes or intergenic regions
164 differing in their nucleotide sequence compared to the inocula). We find a clear and
165 significant distinction between the populations that evolved in the two mouse genotypes (Fig
166 1E, PERMANOVA $P = 0.0022$). The same result was observed when comparing single *de-*
167 *novo* mutated genomic positions between evolved bacterial populations from WT and KO
168 mice (Fig S3, PERMANOVA $P = 0.0016$).

169 ***Single nucleotide polymorphism differentiates evolved bacteria of all inflamed mice from***
170 ***evolved bacteria of healthy mice***

171 To identify candidates for genetic changes that may be specifically selected in an
172 inflamed environment, we focused on parallel mutations (i.e., genes or intergenic regions
173 mutated in at least two mice that were gavaged with an independent inoculum; see Methods)
174 and their associated functions. Analysis of the KEGG pathways encompassed by these loci
175 reveals seven pathways unique to the bacterial populations from inflamed mice (Fig 2A).
176 These pathways include those involved in amino acid metabolism, pyruvate metabolismall of
177 which have been associated with IBD in clinical settings [27,28]. In addition to the pathways
178 affected only in bacterial populations from the inflamed mice, 18 pathways are affected only
179 in populations from healthy mice, and 18 other pathways are mutated in populations from
180 both healthy and inflamed mice (Fig 2A).

181 Univariate analysis reveals that only one particular locus is mutated at significantly
182 higher frequencies in evolved bacterial populations from inflamed than healthy mice
183 (Wilcoxon signed-rank test, corrected $P = 0.001$, Table S9), which is a single nucleotide
184 polymorphism (SNP) (C>T) nine nucleotides upstream of the gene *mprA* (position 3009211)
185 (Fig 2B). It is found in 11/11 KO mice at the endpoint with a frequency between 0.373 and 1,
186 compared to 2/14 WT mice with a frequency between 0.085 and 0.239. Two other mutations
187 are detected in the same intergenic region, although in a few populations only. The bacteria
188 from one WT mouse harbors a C>A mutation at the same position (3009211) with a
189 frequency of 0.052, whereas those from one inflamed mouse harbors a G>T SNP at a nearby
190 position (3009194) with a frequency of 0.611.

191 To further investigate the most frequent C>T mutation, we analyzed its frequency
192 over the course of the experiment (weeks 1, 4, 8, and 12). At week 1 the mutation is not
193 present or below the detection threshold (minimum frequency of 0.05; see Methods), while at

194 week 4, it is observed in 7/11 KO mice with a maximum frequency of 0.616, in comparison
195 to 1/14 WT mice with a frequency of 0.364 (Fig 2C). After a steady increase in frequency at
196 weeks 8 and 12, the mutation reaches fixation or near fixation in 7/11 KO mice and is also
197 present at intermediate frequencies in the remaining 4/11 KO mice (Fig 2C). Importantly, the
198 increase in frequency of the C>T mutation strongly coincides with the increase in
199 inflammation as measured by lipocalin-2 levels, both in KO mice alone and when including
200 all mice (Fig 2C, Fig S4; Spearman's rank correlation rho $P = 0.00005$ for KO mice alone and
201 $P = 3.005e-11$ for all mice).

202 Interestingly, closer inspection of the intergenic region between the hypothetical
203 protein_02879 and the gene *mprA* reveals that this genomic region is a mutational hotspot,
204 with six others positions in this region having mutated over the course of the *in vivo*
205 experiment (Fig S5).

206 Taken together, we identify a C>T change at position 3009211 in the *E. coli* genome,
207 which is a parallel mutation significantly associated with intestinal inflammation. This
208 mutation is located upstream of *mprA* (also known as *emrR*), a transcriptional repressor of
209 several genes, including those encoding the efflux pump EmrAB and AcrAB, and a putative
210 outer membrane porin OmpC (also known as NmpC)[29–31].

211 ***Bacterial populations show significantly different expression profiles in healthy and***
212 ***inflamed mice***

213 To quantify the expression of genes that are part of the *mprA* regulon (*mprA*, *emrAB*,
214 *acrAB*, and *ompC*)[29–31], as well as gain an overall view on differences in gene expression in
215 WT- compared to KO-evolved bacterial populations, we perform metatranscriptomic
216 sequencing of all week 12 bacterial populations. To test for overall differences in the gene
217 expression, we perform a partial least-squares discriminant analysis (PLS-DA) on all genes,
218 using RPKM (Reads per Kilobase per million Mapped Reads) as a proxy for gene expression.

219 We find a clear and significant difference in overall gene expression between populations
220 according to mouse genotype (Fig S6A, PERMANOVA P < 0.00005). Differential
221 expression analysis performed with Deseq2 reveals 2,219 genes that are up- or down-
222 regulated in one of the two conditions (1,022 upregulated for the populations from the
223 healthy gut and 1,197 for the population from the inflamed gut; Benjamini-Hochberg
224 corrected P <0.05, Tab S10). Analysis of the KEGG pathways encompassed by these
225 upregulated genes reveals 25 pathways unique to the bacterial populations from inflamed
226 mice (Fig S6B). These pathways include Ribosome, Aminoacyl-tRNA biosynthesis,
227 Glutathione metabolism, RNA degradation, Folate biosynthesis, Sulfur relay system,
228 Arginine biosynthesis, Protein export, Pantothenate and CoA biosynthesis, and Homologous
229 recombination, among others (Tab S11). Interestingly, *mprA* and *ompC,* which can be
230 putatively regulated by *mprA*[30], are significantly more expressed in the populations that
231 evolved in the inflamed gut (Tab S10; Fig S6C).

232 ***Increase in fitness of evolved bacteria in an inflammatory environment***

233 As parallel mutations are a strong indication of adaptation by natural selection, we
234 hypothesized that the evolved bacterial populations may have a fitness advantage in the
235 environment in which they evolved, and thus next focused on the phenotypes present in the
236 evolved bacterial populations. To test whether evolution in the inflamed mouse gut confers a
237 fitness advantage to *E. coli*, we performed "reciprocal transplant" experiments based on *ex*
238 *vivo* assays using filtered cecal content from inflamed versus non-inflamed mice, collected
239 after sacrifice (referred to subsequently as "*ex vivo* media"). Populations of *E. coli* from fecal
240 samples collected at week 12 from a subset of mice (N = 5 KO mice and N = 5 WT mice)
241 were cultured in *ex vivo* media derived from both inflamed and non-inflamed mice. While no
242 significant difference is observed between bacteria from WT and KO mice when grown in
243 non-inflamed *ex vivo* media (Kruskal-Wallis test P = 0.9168; Fig 3A), bacteria from KO mice

244 grow significantly better than those from WT mice in the inflamed *ex vivo* media (Kruskal-
245 Wallis test $P = 0.009023$). Notably, bacteria from KO mice grow significantly better in the
246 inflamed *ex vivo* media than in the non-inflamed *ex vivo* media (Kruskal-Wallis test $P =$
247 0.0472), while bacteria from WT mice show no difference in growth in the two media
248 (Kruskal-Wallis test $P = 0.4647$). Thus, bacteria that evolved in the inflamed gut possess a
249 fitness advantage in the inflamed gut environment, suggesting that evolution in the inflamed
250 gut results in specific adaptation to that environment.

251 ***Inflamed gut environment displays an altered metabolomic profile***

252 To gain a better understanding of the environment to which these bacteria are adapted,
253 we performed metabolomic analysis of fecal samples spanning the experimental time course
254 (weeks 1, 2, 5, 6, 10, and 12) using 1H-NMR in mice from one of the two experiments. While
255 WT and KO mice initially display very similar fecal metabolomes (PERMANOVA $P =$
256 0.754), with time, the fecal metabolic composition begins to vary concurrently with the onset
257 of inflammation and the frequency of the C>T SNP upstream of *mprA* (Fig 3B, 1B, 2C). By
258 week 12 of the evolution experiment, WT and KO mice exhibit notable differences in their
259 fecal metabolomes, as revealed by PLS-DA (PERMANOVA $P = 0.001$; Fig 3B, Fig S7).
260 Among the 77 metabolite features initially found in the samples from week 1, none show
261 significantly different abundances between the WT and KO mice (Table S12). In contrast, in
262 the week 12 samples, 59 of the 77 detected features exhibit significant differences in
263 abundance between WT and KO mice (Benjamini-Hochberg corrected $P < 0.05$; Table S13).
264 Notably, 42 are significantly more abundant in KO mice than in WT mice, including all
265 detected amino acids that were significantly enriched in KO mice based on KEGG pathway
266 analysis of parallelly mutated loci. Among the 17 enriched features in the WT mice, most are
267 putatively annotated as (poly-)saccharides (Fig S8). Notably, variations in fecal metabolic
268 composition at week 12 could arise from changes in both the host, linked to inflammation-

269 related changes, and the bacterial population, associated with bacterial adaptation to
270 inflammation.

271 ***Phenotypic profiling of evolved bacteria compared to ancestor***

272 Having established that the environment in which the bacteria evolved significantly
273 differs according to the mouse genotype, we next focused on specific bacterial traits that may
274 have changed as a consequence of adaptation. Accordingly, we tested the metabolic activity
275 of the *E. coli* populations using the Biolog GENIII test panel, which comprises 94 unique
276 biochemical tests, including a range of compounds (e.g., sugars, amino acids, and short-chain
277 fatty acids), conditions (e.g., different pH and salt concentrations), and chemical sensitivities
278 (e.g., antibiotics; see Methods). Similar to the pattern observed for the fecal metabolome, the
279 overall bacterial metabolic activity across all tested conditions is similar among populations
280 derived from the WT and KO mice at week 1 of the experiment (PERMANOVA, $P = 0.519$;
281 Fig S9), as also evidenced by the overlapping of the groups in the PLS-DA based on the
282 overall metabolic activity observed in the BIOLOG GENIII tests (Fig 3C). However, by
283 week 12, the overall pattern of metabolic activity across all tested conditions significantly
284 differs between the bacteria from KO and WT mice (PERMANOVA, $P = 0.005$, Fig S9).
285 These results suggest that adaptation to the inflamed intestine results in significantly altered
286 bacterial metabolism and the ability to grow in the presence of different inhibitors. Among
287 the compounds included in this screen, bacteria from WT and KO mice from week 1 showed
288 significantly different metabolic activity in only one compound (Table S14). In contrast,
289 bacteria from WT and KO mice at week 12 display significantly different metabolic activities
290 in the presence of 31 compounds (Wilcoxon signed-rank test, corrected $P < 0.05$; Table S15,
291 Fig S10).

292 To determine whether the differences in growth observed among the 31 compounds at
293 week 12 may be related to the altered metabolomic environment of inflamed mice, we

294 compared our BIOLOG GENIII results to the compounds found to be enriched in the fecal
295 metabolome of the KO mice. Interestingly, metabolomics analysis revealed a significant
296 enrichment of the amino acid histidine in the feces of KO mice compared to that of WT mice
297 (Fig S8). In our *in vitro* metabolic assay, we found that bacteria adapted to the inflamed
298 intestine had a significantly higher ability to metabolize histidine than bacteria adapted to the
299 healthy intestine (Fig S10). Thus, adaptation to an environment enriched in histidine may
300 have conferred a higher metabolic activity in the presence of this amino acid.

301 To further explore how the results of our *in vitro* phenotypic analyses may relate to
302 the fecal metabolomic profile observed *in vivo*, we performed a shortest path analysis on the
303 metabolic network of the genome-scale metabolic model of *E. coli* NC101 [32] using
304 metabolomic data and data from the *in vitro* metabolic activity screen (BIOLOG plates; see
305 Methods). Pairs of compounds from the two datasets that are converted easily to each other
306 by means of pathway length include glutamate and L-arginine (Fig 3D, Table S16).
307 Glutamate is significantly more abundant in the feces of the inflamed mice (Fig S8), whereas
308 bacteria adapted to the inflamed intestine are capable of significantly higher metabolism in
309 the presence of L-arginine (Fig S10). This result suggests that the bacteria may be converting
310 arginine to glutamate, resulting in the enrichment of glutamate in KO mice (Fig 3D, Table
311 S16). A second pair of compounds showing the same pattern are taurine and L-arginine.
312 However, analysis of the potential pathways between these compounds through flux
313 variability analysis revealed that taurine cannot be produced by *E. coli* NC101 under any of
314 the tested conditions (Fig S11). Additionally, taurine abundance increased steadily over time
315 only in KO mice (Fig S12). Thus, taurine is most likely to be produced by the host.

316 Finally, we examined 31 significant differences in metabolic activity observed
317 between bacteria from WT and KO mice at week 12, in light of their potential clinical value.
318 A first compound of interest is N-acetyl beta-D mannosamine (NADM), which is a precursor

319 to sialic acid and has been shown to promote *E. coli* colonization of inflamed gut [33]. Our *E.*
320 *coli* populations show higher levels of metabolic activity in the presence of NADM after
321 adaptation to the inflamed mouse gut. In contrast, *E. coli* evolved in the non-inflamed mouse
322 gut show no such change (Fig 4). These findings suggest that increased virulence may occur
323 in the context of adaptation to an inflamed environment.

324 Another interesting candidate is lithium chloride, which is known to have anti-
325 inflammatory effects via the inhibition of a key host regulator of inflammation, glycogen
326 synthase kinase-3 beta [34]. In our experiment, bacterial populations evolved in WT mice
327 display improved metabolic capacity in the presence of lithium chloride compared to the
328 ancestor, while no such change is observed among those evolved in the KO mice. Thus, our
329 results suggest that an inflamed intestinal environment may prevent the acquisition of this
330 phenotype in *E. coli*.

331 A final promising category of candidates are antibiotics, including fusidic acid,
332 vancomycin, and lincomycin. When considering the loading plot of the PLS-DA of our
333 Biolog GENIII data (Fig S13; reporting which compounds contribute the most to the
334 separation between groups), all three of these antibiotics contributed to the overall significant
335 difference in the metabolic activity of the bacteria from WT and KO mice (Fig 3C, Fig S13).
336 Furthermore, fusidic acid is also significantly different between bacteria from the two mouse
337 genotypes in the univariate analysis (Wilcoxon signed-rank test, corrected $P < 0.05$). Fusidic
338 acid is an antibiotic that targets gram-positive bacteria, and is commonly used to treat skin
339 infections [35]. Interestingly, it was also shown to be effective in reducing disease activity in a
340 small number of patients with Crohn's disease, which is thought to be due to its
341 immunosuppressive properties [36,37]. We observe *E. coli* to display decreased metabolic
342 activity in the presence of fusidic acid after adaptation to the inflamed intestine but increased
343 metabolic activity after adaptation to the healthy intestine. These results suggest a potential

344 trade-off between adaptation to inflammation and resistance to fusidic acid, where *E. coli*
345 adapted to inflammation also show lower resistance to fusidic acid.
346 In summary, we observe widespread phenotypic differences among the bacterial
347 populations that evolved in the inflamed intestines of KO mice compared to non-inflamed
348 WT mice. These results relate to differences in the metabolome between these two intestinal
349 environments and include phenotypes that carry the potential for exploitation in a clinical
350 setting.

351 **Discussion**

352 In this study, we describe the findings of an *in-vivo* bacterial evolution experiment
353 using a gnotobiotic mouse model of IBD. We find that *E. coli* evolved in the inflamed mouse
354 gut accumulated specific genetic changes and that these changes confer a fitness advantage in
355 the inflamed intestinal environment, which significantly differs in its metabolome.
356 Furthermore, we show that *E.coli* populations in the gut of healthy and inflamed mice have a
357 distinct metatranscriptomic profile. Finally, we showed that adaptation to the inflamed
358 intestine resulted in several phenotypic differences that may be clinically relevant, such as
359 differential tolerance to antibiotics.
360 Recent studies have highlighted how strain-level changes in members of the gut
361 microbiome can play a crucial role in the adaptation of the gut microbiome to novel
362 conditions [14,38,39]. However, the effects of inflammation on the evolution of gut commensals
363 remain largely unexplored. Barreto et al. (2020) followed the adaptation of *E. coli* in mice of
364 different ages *in vivo* [14]. They showed that the aged mouse gut, which also showed high
365 levels of inflammation, was a more stressful environment for *E. coli*, resulting in a higher
366 number of mutations and more severe selective pressure on commensals, particularly in
367 bacterial loci associated with stress-related functions. Notably, we find no difference in the
368 number of mutations acquired by *E. coli* in inflamed mice, suggesting that other factors

369 associated with aging may contribute to the increased bacterial mutation rate observed by
370 Barreto et al. (2020) [14].
371 More recently, Tawk et al. (2023) conducted a study of mice monocolonized with
372 *Bacteroides thetaiotaomicron* that were subsequently infected with *Citrobacter rodentium*
373 and developed inflammation. In this setting, a single-nucleotide variant of *B.*
374 *thetaiotaomicron*, which had a higher tolerance to oxidative stress than the ancestral variant,
375 underwent selective sweeps and dominated the intestinal community [39]. Although the
376 experimental setup and duration of inflammation differ between this study and the current
377 study, our candidate mutation is also known to be associated with oxidative stress [40]. This is
378 consistent with the observations of Barreto et al. (2020) and Tawk et al. (2023) [14,39],
379 suggesting that oxidative stress is a key selective pressure in an inflamed environment.
380 Moreover, oxidative stress plays a major role in the pathophysiology of IBD [41]. Interestingly,
381 this is also confirmed by our metatranscriptomic analysis. In particular, 14 of the genes
382 upregulated in KO mice belong to the pathway of glutathione metabolism (eco00480), and
383 previous studies demonstrated that glutathione metabolism is involved in protection against
384 oxidative stress [42,43]. In addition, Sakamoto et al. reported *mprA* to be involved in resistance
385 to oxidative stress, together with the activity of *gshA* (glutathione synthase), which is also
386 upregulated in our populations[40]. Additionally, our metatranscriptomic data confirm the
387 findings of Tawk et al., suggesting a role for vitamin B6 metabolism [39]. We observe not only
388 the upregulation of nine genes belonging to the vitamin B6 metabolism (eco00750), but also
389 a significantly higher concentration of aspartate, a substrate of vitamin B6-dependent
390 enzymes, in the feces of the inflamed mice[39].
391 Importantly, many of our findings are consistent with the observations made in
392 clinical IBD settings. First, the KEGG pathways affected by parallel mutations specific to the

393 inflamed mice (Fig 2A) include D-amino acid-, pyruvate-, and thiamine metabolism. This is
394 in line with previous reports that the basic metabolism is reduced in IBD [27,44].
395 Second, the metabolomic profiling of the fecal samples reveals that KO mice have
396 significantly higher levels of many amino acids, which was also reported in IBD patients [45].
397 Furthermore, the results of our shortest path analysis suggest that bacterial production of
398 glutamate from arginine may underlie the enrichment of glutamate in the inflamed gut.
399 Although taurine-arginine was also one of the shortest paths we found, taurine could not be
400 produced by *E. coli* according to the flux variability analysis. Thus, taurine is most likely to
401 be produced by the host. Taurine is known to be a promoter of colonization resistance, and
402 infection has been shown to prime the microbiota against subsequent infections by inducing
403 host production of taurine [46]. Indeed, taurine was also reported to ameliorate inflammation in
404 rat models of inflammation [47]. Furthermore, taurine is a substrate for the microbiota-driven
405 production of hydrogen sulfide [48], and arginine is a precursor to polyamines that can protect
406 against reactive species such as hydrogen sulfide [49]. Thus, bacterial adaptation for improved
407 metabolic activity in the presence of arginine may be a response to the host-induced
408 inflammatory changes in the intestine.
409 Third, *E. coli* adapted to the inflamed mouse gut also showed some clinically relevant
410 phenotypes (Fig 4). N-acetyl beta-D mannosamine (NADM) is a precursor of polysialic acid,
411 a pathogenic determinant, and studies have shown that it can promote colonization of the
412 inflamed intestine by pathogenic *E. coli* [33,50]. As NADM is a crucial player in mediating
413 pathogenic activity in the inflamed intestine, the improved metabolic activity of
414 inflammation-adapted *E. coli* observed in the presence of NADM may be a phenotype
415 associated with virulence. This is consistent with reports of virulence-associated phenotypes,
416 such as hypermotility, selected during the evolution of an adherent-invasive *E. coli* in the
417 inflamed mouse gut [13]. Furthermore, lithium chloride is known to inhibit the activity of

418 glycogen synthase kinase 3-β, a master regulator of host chronic intestinal inflammation
419 mediated by toll-like receptors, and has been used as a treatment in a mouse model of IBD
420 [34,51]. However, the effect of lithium on the microbiome has not yet been elucidated. *E. coli*
421 tolerance to lithium ions is regulated through antiporters, and proline has been shown to
422 induce the uptake of lithium ions by *E. coli* [52,53]. Our finding that adaptation to the healthy
423 mouse intestine confers improved metabolic capacity in the presence of lithium chloride,
424 while adaptation to the inflamed intestine does not (Fig 4), implies that lithium may affect
425 both the host and microbiome. This may also imply that adaptation to the healthy intestine
426 affects the antiporter-dependent detoxification system of *E. coli*, resulting in improved ion
427 tolerance.

428 Lastly, we found that bacterial adaptation to the inflamed gut decreases metabolic
429 activity in the presence of fusidic acid, while adaptation to the healthy mouse gut improved
430 metabolic activity in the presence of fusidic acid (Fig 4). Fusidic acid is an antibiotic with T
431 cell-specific immunosuppressive effects that also stimulate gastric mucus secretion.
432 Furthermore, it was successfully applied to alleviate inflammation in rats, as well as to treat
433 selected patients with Crohn's disease for whom conventional treatment was ineffective [36,37].
434 However, the effect of fusidic acid on the gut microbiome in IBD has not yet been studied.
435 Our results imply that bacterial adaptation to the inflamed gut can result in a trade-off for
436 resistance to fusidic acid. Importantly, such trade-offs are a fundamental concept in
437 evolutionary medicine, where increased fitness in one context results in a consequent
438 decrease in fitness in another context, and are proposed as possible potent therapeutic
439 strategies against antibiotic resistance and cancer [18,54]. Thus, the therapeutic effect of fusidic
440 acid observed in patients with CD is due to trade-offs in microbiome adaptation to the
441 inflamed gut and/or its immunosuppressive effects on the host. Interestingly, it is known that
442 lipocalin-2 plays a role in iron-sequestration, which has been reported to have a role in

443 antibiotic resistance and sensitivity[55]. It is thus worth noting that there is no enrichment of
444 genes involved in iron metabolism among the mutated genes in the populations evolved in the
445 inflamed gut, as well as among the upregulated genes in these populations.

446 Current treatment options for IBD are largely limited to the treatment of inflammation
447 with a chronic risk of relapse. Corticosteroids, aminosalicylates, and immunosuppressive
448 agents are the conventional drugs of choice, but the safety and efficacy of novel emerging
449 strategies remain unclear (reviewed in [56]). Given that disease-specific aspects of the
450 microbiome have been shown to remain stable over long periods in IBD patients despite
451 treatment [57], a persistent microbial influence on the intestinal environment may be a key risk
452 factor for relapse. Thus, our results highlight new avenues of research involving evolution-
453 informed therapeutic strategies that exploit trade-offs to either prevent adaptation to
454 inflammation and/or help restore desirable ancestral traits in the microbiome.

455 While our results provide valuable insights into the potential role of evolution-
456 informed therapeutic strategies, it is important to acknowledge that it remains unknown
457 whether the same or similar genotypic and phenotypic changes would be observed in the
458 context of a complex microbial community as present in the human gut microbiome. Future
459 work should therefore include similar *in vivo* evolution experiments using a complex or
460 synthetic microbial community.

461 **Methods**

462 ***Bacterial strains***

463 *E. coli* NC101 strain was obtained from Balfour Sartor, University of North Carolina,
464 Chapel Hill, NC, USA [58]. *Escherichia coli* NC101 is a mouse strain isolated from the
465 intestine of a WT 129S6/SvEv mouse raised under specific-pathogen-free (SPF) conditions
466 [58]. The strain was cultured at 37 °C in Luria Bertani (LB) medium with continuous shaking.

467 The ancestor strain for the *in vivo* experiment was obtained by plating the overnight culture
468 on LB agar and picking single colonies to be used as inocula for the *in vivo* evolution
469 experiment.

470 ***Mouse model***

471 Two independent experiments were conducted to study *E. coli* adaptation to the
472 inflamed gut (Table S1). In the first experiment, "Exp1", a single inoculum was used for all
473 mice. In order to ensure that mutations present in a common inoculum could not be falsely
474 identified as "parallel" mutations, the second experiment, "Exp2" was performed with
475 independent inocula for each mouse. Accordingly, our definition of a parallel mutated gene
476 requires it to be mutated in at least two mice that were gavaged with a different inoculum.
477 Germ-free (GF) C57BL/6NTac (WT) and C57BL/6NTac-Il10em8Tac (KO) male mice were
478 purchased from Taconic Biosciences (Silkeborg, Denmark) and housed in the Germ-Free
479 Animal Facility at the Max Planck Institute for Evolutionary Biology (Ploen, Germany). GF
480 mice were maintained in sterile isolators (MB-10, Quip Laboratories, Delaware, USA) and
481 fed sterilized 50 kGy V1124-927 Sniff (Soest, Deutschland). The animals were allocated to
482 independent cages with a maximum of four mice per isolator until they reached an age of 12
483 weeks. Detailed information regarding the mice used in this study is presented in Table S1.
484 Initially, 19 WT and 15 KO mice were mono-colonized with the *E. coli* NC101 strain. Only
485 mice that survived the duration of the experiment (12 weeks; N = 14 WT mice and N = 11
486 KO mice) were included in the study. The study was performed in accordance with the
487 approved animal protocols and institutional guidelines of the Max Planck Institute for
488 Evolutionary Biology, Plön. Mice were maintained, and experiments were performed in
489 accordance with FELASA guidelines and German animal welfare law (Tierschutzgesetz § 11;
490 permits from Veterinäramt Kreis Plön: 1401-144/PLÖ-004697 and Veterinäramt Kreis Kiel:
491 244-509017/2018(107-11/18)).

492 The strains used as inocula were diluted in sterile PBS, and 200 µl (equivalent to
493 1x10^8 bacteria) were gavaged using a sterile gavage needle (Reusable Feeding Needles
494 18G, Fine Science Tools, Heidelberg, Deutschland). Fecal pellets were collected in a sterile
495 manner twice a week to study the evolution of *E. coli* for a total of 24 samples collected per
496 mouse and once a week for metabolomic investigation. An overview of the sampling plan is
497 presented in Fig 1A.

498 ***Histopathological evaluation***

499 Mice were sacrificed at week 12, and colon tissue was collected and arranged to form
500 a Swiss-roll [59]. Hematoxylin and eosin-stained sections of colonic tissue Swiss rolls were
501 scored by two independent researchers in a blinded manner using the scoring system
502 described by Adolph et al. (2013) [60]. The score is composed of five sub-scores: mononuclear
503 cell infiltrate, crypt hyperplasia, epithelial injury or erosion, polymorphonuclear cell
504 infiltrates, and transmural inflammation. Each of the first four sub scores was awarded a
505 score from 0 to 3, whereas transmural inflammation was scored from 0 to 4, with a higher
506 score indicating a more severe level of inflammatory activity. The sum of the sub scores was
507 then multiplied by a factor based on the percentage of affected bowel length (1= < 10%; 2=
508 10-25%; 3= 25-50%; 4= >50%).

509 ***Feces processing***

510 Feces weight and consistency were recorded. Feces were homogenized in 1.5 ml
511 sterile PBS on a horizontal vortexer (Vortex Mixer Modell Vortex-Genie® 2, Scientific
512 Industries, Bohemia, NY, USA) at maximum speed for 30 min, then separated in three
513 aliquots of 500 µl. Each aliquot was centrifuged at 10,000 rpm for 5 min. The supernatants
514 were transferred to a new tube and stored at -20 °C for subsequent lipocalin-2 concentration

515 measurement. One pellet aliquot was resuspended in 500 µl of PBS and used to prepare a 12-
516 point 1/10 dilution series in a 96-well plate. Ten µl were plated onto an LB agar plate. Plates
517 were incubated overnight at 37°C and colonies were counted to estimate the bacterial load.
518 The bacterial load in the fecal samples was calculated by normalizing CFU counts by wet
519 feces weight. The second pellet aliquot was resuspended in 1 ml RNAlater and stored at +4
520 °C for 24 h, after which the tube was centrifuged at 10,000 rpm for 5 min to remove the
521 RNAlater, and the pellet was stored at -20 °C for subsequent nucleic acid extraction and
522 sequencing. The final pellet aliquot was resuspended in 500 µl of LB containing 20%
523 glycerol and stored at -70 °C for further phenotypic investigation.

524 ***Lipocalin-2 quantification***

525 Lipocalin-2 concentration in the supernatants was measured using the commercial kit
526 Mouse Lipocalin-2/NGAL DuoSet ELISA (R&D Systems, Minneapolis, MN, USA) for
527 mouse Lipocalin-2 (DY1857). Testing was performed according to the manufacturer's
528 instructions. The samples were diluted 1:10 and added to the plate. The optical density of
529 each well was determined using a plate reader (SPARK, Tecan, Tecan, Männedorf,
530 Switzerland) at 450 and 540 nm. Lipocalin-2 concentrations were normalized to the weight of
531 feces for each sample.

532 ***Shotgun sequencing***

533 Total DNA and RNA were extracted using the ZymoBIOMICS DNA/RNA Mini Kit
534 (Zymo Research, Freiburg, Germany), following the manufacturer's instructions from fecal
535 pellets collected at weeks 1, 4, 8, and 12, as well as from the *E. coli* NC101 cultures that
536 served as inocula. Shotgun metagenomic sequencing was performed on four Illumina

537 Nextseq (HighOutput 300 cycles) sequencing runs at the Max Planck Institute for
538 Evolutionary Biology (Plön, Germany).
539 Raw reads were filtered and trimmed to ensure good quality using Cutadapt (version
540 3.2, [61]). First, any pair containing Ns, homopolymers (10 nucleotides or more), or those
541 longer than 151 bp were discarded. Sequences were trimmed with a quality cutoff of 25 at
542 both ends for both reads, Illumina adapters were removed, and sequences shorter than 50 bp
543 were discarded. Good quality sequences were then filtered to exclude mouse sequences
544 (mouse_C57BL) using KneadData [62]. A final filter was applied to remove any adapter
545 leftovers using Trimmomatic [63] and sequences shorter than 105 bp were discarded. Mutations
546 were identified using Breseq [64] by comparing the obtained metagenomes with the reference
547 genome of *E.coli* NC101 (PRJNA596436) using default options (i.e. mutations identified by
548 a threshold frequency > 0.05) and by subtracting the mutations that were detected in the
549 respective inoculum. Gdtools was used to compare mutations in the samples.
550 ***Metatranscriptomics***
551 Depletion of rRNA from extracted RNA was performed using QIAseq FastSelect -
552 5S/16S/23S (Qiagen). Samples were incubated at 89°C for 8 minutes. Libraries for
553 metatranscriptomics were prepared using the Illumina TruSeq® Stranded mRNA Library
554 Prep Kit (Illumina) according to the manufacturer's instructions. Shotgun metatranscriptomic
555 sequencing of week 12 fecal samples was performed on an Illumina NextSeq 500/550 using
556 the HighOutput Kit v2.5 (75 cycles).
557 Quality control and trimming were performed as described above for shotgun
558 sequencing. Gene expression in the evolved population was calculated in Geneious (v
559 2022.2.1; https://www.geneious.com) by mapping reads to the reference genome of *E.coli*
560 NC101 (PRJNA596436). Differential expression was calculated using DeSeq2[65] as

561 implemented in Geneious, using the parametric model and by assigning the conditions to
562 "WT-" or "KO-evolved".

563 ***Measurement of the metabolic activity of bacteria***

564 Biolog GENIII MicroPlates (Biolog, Hayward, CA, USA) was used to investigate the
565 metabolism of evolved populations. Evolved populations stored in glycerol were inoculated
566 onto the Inoculation Fluid-A (IF-A) provided by the manufacturer such that the OD_{600} was
567 between 0.02-0.05. After adjusting the OD_{600}, the inoculated IF-A was shaken well and
568 distributed into a Biolog GENIII MicroPlate (100 µl in each well). The plate was then
569 covered with a sterile Breathe-Easy membrane (Sigma-Aldrich, St. Louis, MO) and placed in
570 a plate reader (SPARK, Tecan, Männedorf, Switzerland) at a preset temperature of 37 °C.
571 The plate reader was then run with the following parameters: temperature: 37 °C, shaking:
572 250 rpm, OD_{590} measurement: every 15 min, total running time: 36 h. From the OD_{590}
573 measures, area under the curve (AUC) was used as a proxy for metabolic activity. The Biolog
574 assay was repeated for populations from fecal samples collected at weeks 1 and 12 from all
575 25 mice, with two replicates each.

576 ***Ex vivo assay***

577 The cecal content was collected from each mouse during dissection at the end of the
578 second experiment. The amount of cecal content from each mouse was different based on the
579 amount in the cecum at the time of dissection. Sterile PBS was added to the cecal content,
580 and the volume was adjusted based on the amount of cecal content collected from each
581 mouse (20 mg/ml). The protocol was adapted from Kitamoto et al. (2020) [66]. The PBS-cecal
582 content mixture was centrifuged twice (once at 500*g* for 5 min and again at 10000*g* for 5
583 min) and then filter-sterilized through a 0.2 µm filter. The *ex vivo* medium from each mouse
584 was mixed well and 100 µl was spread onto an LB agar plate to ensure that they were sterile.

585 *Ex vivo* media from all healthy mice were pooled, as were the *ex vivo* media from all
586 inflamed mice, resulting in two *ex vivo* media. Populations from fecal samples collected at
587 week 12 from a subset of mice (n = 5 KO and n = 5 WT mice) were inoculated into the *ex*
588 *vivo* media and incubated in the TECAN Spark plate reader at a preset temperature of 37 °C.
589 The plate reader was then run with the following parameters: temperature: 37 °C, shaking:
590 250 rpm, OD_{600} measurement: every 15 min, total running time: 36 h. From the OD_{600}
591 measures, area under the curve (AUC) was used as a proxy for growth.

592 ***Metabolomic evaluation of the fecal pellets***

593 During the second experiment, samples for metabolomic investigation were collected
594 once a week and snap-frozen in liquid nitrogen. Samples were stored at -70 °C and delivered
595 at Helmholtz Center Munich for metabolomic investigation. A non-targeted metabolomics
596 approach of mouse fecal samples was undertaken using NMR spectroscopy. To extract the
597 aqueous metabolites, we homogenized 2-3 fecal pellets in 1 mL H_2O using ceramic beads
598 (NucleoSpin, Macherey–Nagel, Dueren, Germany) and a TissueLyser (Qiagen, Hilden,
599 Germany), mixing the sample for 3 × 30 s at 4,500 rpm with a 10 s cooling break (< 0°C).
600 Subsequently, the homogenate was centrifuged (13,000 rpm for 10 min at 4 °C), the
601 supernatant evaporated using a SpeedVac, and the dried extract reconstituted in 200 µL NMR
602 buffer (10% D_2O, 100 mM phosphate buffer with 0.1% trimethylsilyl-tetradeuteropropionic
603 acid (TSP), pH 7.4). Samples were transferred to 3 mm NMR tubes, and immediate NMR
604 analysis was performed in a randomized order with a Bruker 800 MHz spectrometer
605 operating at 800.35 MHz equipped with a Bruker SampleJet for sample cooling (283 K) and a
606 QCI-cryogenic probe. A standard one-dimensional pulse sequence (noesygppr1d) provides an
607 overview of all molecules. The acquisition parameters were as follows: water suppression
608 irradiation during recycle delay (2 s), mixing time of 200 ms, 90 °pulse of 12.5 µs. We
609 collected 512 scans of 64 K data points with a spectral width of 12 ppm. The software

610 TopSpin 3.6 (Bruker BioSpin, Ettlingen, Germany) was used for processing, i.e., Fourier
611 transformation, manual phasing, baseline correction, and calibration to TSP (δ 0.00). Data
612 were imported into Matlab software R2011b (Mathworks, Natick, MA, USA) and further
613 processed, i.e., the water region was removed, baseline adjusted [67] and spectra normalized [68].
614 Relative quantification of metabolites was performed using the peak heights of selected peaks
615 and compounds identified as described in our published workflow [69].

616 ***Shortest path analysis***

617 For the shortest path analysis, we used the metabolic model reconstructed using the
618 AGORA2 resource for the human microbiome [32]. The model was translated into a graph with
619 metabolites as nodes, and the reactions converting metabolites into one another as edges. The
620 shortest path analysis was performed using the Dijkstra algorithm implemented in the igraph
621 package (1.3.5) of R (4.2.2) [70,71]. To avoid shortcuts through the network using cofactors as
622 intermediate compounds, the edges were weighted by the sum of degree of the nodes it
623 connected, as suggested by Faust et al. [72]. For each compound from the *in vitro* screen, we
624 calculated the set of shortest paths to all other metabolites in the model. Each value in the set
625 was the average shortest path of the five shortest paths between two metabolites, which was
626 performed to account for uncertainties in pathway calculation based only on the network
627 properties. For our analysis, we only considered pathways between compounds from the two
628 datasets, which were among the shortest 5% of pathways in a pathway set.

629 ***Prediction of possible conversions between metabolites***

630 We wanted to understand whether the altered metabolic capabilities observed in the Biolog
631 plates or the changed environmental conditions observed in the metabolomic data, together
632 with the metabolism of *E. coli* could contribute to the observed changes in the metabolomic

633 data between KO and WT mice. To this end, we performed flux variable analysis (FVA) on
634 the metabolic model for E. coli NC101 (retrieved from AGORA2) [32]. We defined every
635 significantly detected metabolite in the Biolog experiment or the metabolomic data set as a
636 possible source metabolites, while the metabolites from the metabolomic data set were
637 defined as target metabolites. Metabolites found in the metabolomics are those known to be
638 present *in vivo*. Compounds found to be significantly differentially metabolized in the Biolog
639 assay are those that we know the evolved bacteria are capable of metabolizing. By using the
640 sum of these as the source and the detected metabolites as the target, we aimed to capture as
641 many of the possible conversions as possible to help explain the composition of the *in vivo*
642 environment and the role of bacterial metabolism in shaping it. For the simulation
643 background, we employed a minimal medium (Table S13), removed D-Glucose, and adjusted
644 the oxygen level according to the conditions tested (anoxic = 0 mmol h^{-1} gDW^{-1},
645 microaerobic = 1 mmol h^{-1} gDW^{-1}, aerobic = 10 mmol h^{-1} gDW^{-1}). For the simulation, we
646 added each source metabolite individually to the growth medium (100 mmol h^{-1} gDW^{-1}) and
647 calculated the maximum production rates of the target metabolites, assuming that at least
648 50% of maximum growth rates were achieved. We considered a maximum flux of $>1e^{-6}$ as
649 the possible production of the target metabolite from the source metabolite. FVA was
650 performed in cobrapy [73] and analyses were performed using the data.table and ggplot2
651 packages for R.

652 ***Statistical investigation***

653 Statistical analyses were performed using packages in RStudio 2023.03.0+386. For
654 PERMANOVA analyses, adonis was used [74] on Bray-Curtis distances of the data [75] and
655 mixomics was used for PLS-DA [76]. AUCs were calculated using desctools [77].

656 **Acknowledgments**

657 We are grateful to Balfour Sartor for providing the NC101 *E. coli* strain, the MPI-Plön mouse
658 team for support with animal experiments, Britt Marie Hermes for support in manuscript
659 preparation, and Wael Elhenawy and Isabel Gordo for their helpful and constructive
660 discussions. The authors acknowledge the use of ChatGPT for the purpose of supporting the
661 drafting of material for the introduction section.

662 **Funding**

663 This study was supported by the Deutsche Forschungsgemeinschaft (DFG) Research Unit
664 FOR5042 "miTarget – The Microbiome as a Target in Inflammatory Bowel Disease"
665 (subprojects P10, Z, and INF) and Cluster of Excellence 2167 "Precision Medicine in
666 Chronic Inflammation" (grant no. EXC2167). RU was funded by the International Max-
667 Planck Research School for Evolutionary Biology (IMPRS EvolBio). Work in the
668 Unterweger group is funded by the German Federal Ministry for Education and Research
669 (grant 01KI2020).

670 **Disclosure statement**

671 The authors report there are no competing interests to declare.

672 **Data availability statement**

673 *Escherichia coli* NC101 reference genome is available under Bioproject number
674 PRJNA596436. Shotgun metagenomic sequencing of the inocula and evolved

675 populations and metatranscriptomic of the populations at week 12 are available with
676 Bioproject number PRJNA1012288.

677 **Author contributions**

678 MV, DU, and JB conceptualized the study; RU, NAA, MV, SH, MAG, OV, SK and DU
679 performed experiments; RU, NAA, MV, SH, FT, JH, and PR analyzed the data; JT and CK
680 performed the metabolic modeling; RU, NAA, and AD performed the statistical analyses.
681 RU, NAA, DU, and JB wrote the first draft of the manuscript. All coauthors revised the
682 manuscript and agreed to its publication.

683

684

685 **Figures captions**

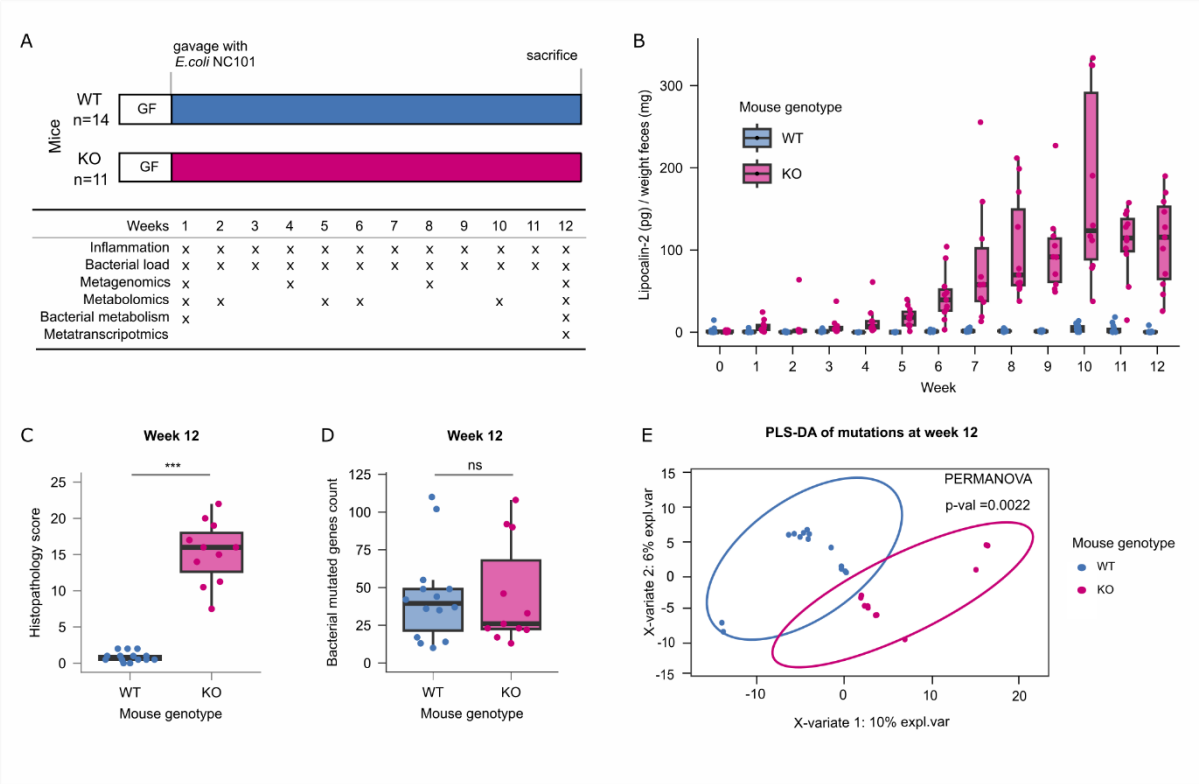

686

687 **Figure 1. Application of a mouse model of IBD to test the effect of gut inflammation on**

688 **the evolution of NC 101**

689 **A** Schematic of the experimental setup. Germ-free WT and *Il10*$^{-/-}$ mice were monocolonized

690 with *E. coli* NC101. Fecal samples were collected from each mouse at the indicated time

691 points and analyzed as described. **B** Fecal lipocalin-2 levels from the WT and *Il10*-/- mice.

692 Lipocalin-2 was measured using the Mouse Lipocalin-2/NGAL DuoSet ELISA and

693 normalized to feces weight. Each dot represents one mouse at each sampling point. Results of

694 Wilcoxon signed-rank test of lipocalin-2 concentrations at each time point are reported in

695 Table S3. Differences were considered statistically significant at Benjamini-Hochberg-

696 corrected P <0.05. **C** Boxplots of the histopathology scores of the colon tissue of mice after

697 sacrifice at the end of the experiment. Each dot represents a single mouse. Differences were

698 considered statistically significant using the Kruskal-Wallis H test at Benjamini-Hochberg-

699 corrected P <0.05. **D** Number of *de-novo* mutations in the bacterial populations at week 12 in

700 WT and KO mice compared with the reference genome. Each dot represents a bacterial
701 population from a single mouse. Differences were considered statistically significant using
702 the Kruskal-Wallis H test at Benjamini-Hochberg-corrected $P < 0.05$. **E** Partial least squares-
703 discriminant analysis of the *de-novo* mutated genes in the evolved populations of *E. coli*
704 NC101 at week 12 in WT and KO mice compared to the reference genome. Differences were
705 considered statistically significant at a PERMANOVA $P < 0.05$.
706

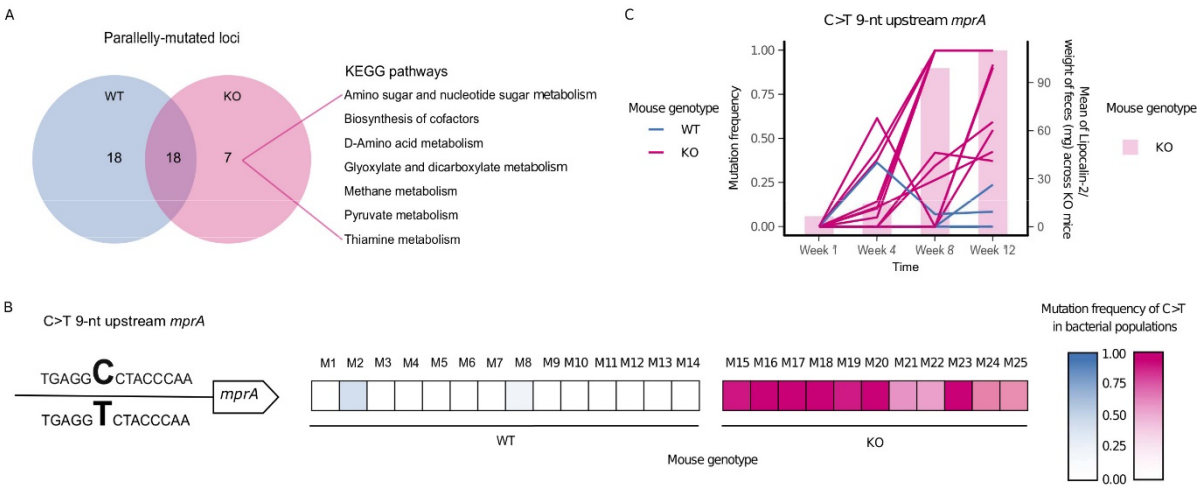

Figure 2. Parallel evolution of *E. coli* in inflamed mice revealed a disease-specific genetic signature A Parallelly mutated genes were classified based on KEGG pathways; **B** An intergenic C>T mutation 10-nt upstream of *mprA* was the unique parallel mutation significantly more abundant in populations evolved in the inflamed gut (Wilcoxon signed-rank test Benjamini-Hocheberg corrected $P < 0.005$). The heatmap shows the frequency of the mutation in bacterial populations from each mouse. **C** Mutation frequency (left axis) of the intergenic C>T mutation 10-nt upstream of *mprA* and mean of lipocalin-2 concentrations across KO mice at different timepoints during the *in-vivo* evolution experiment. Each line represents a population from a single mouse. Each bar represents the mean value of the normalized concentration of lipocalin-2 in fecal samples from KO mice.

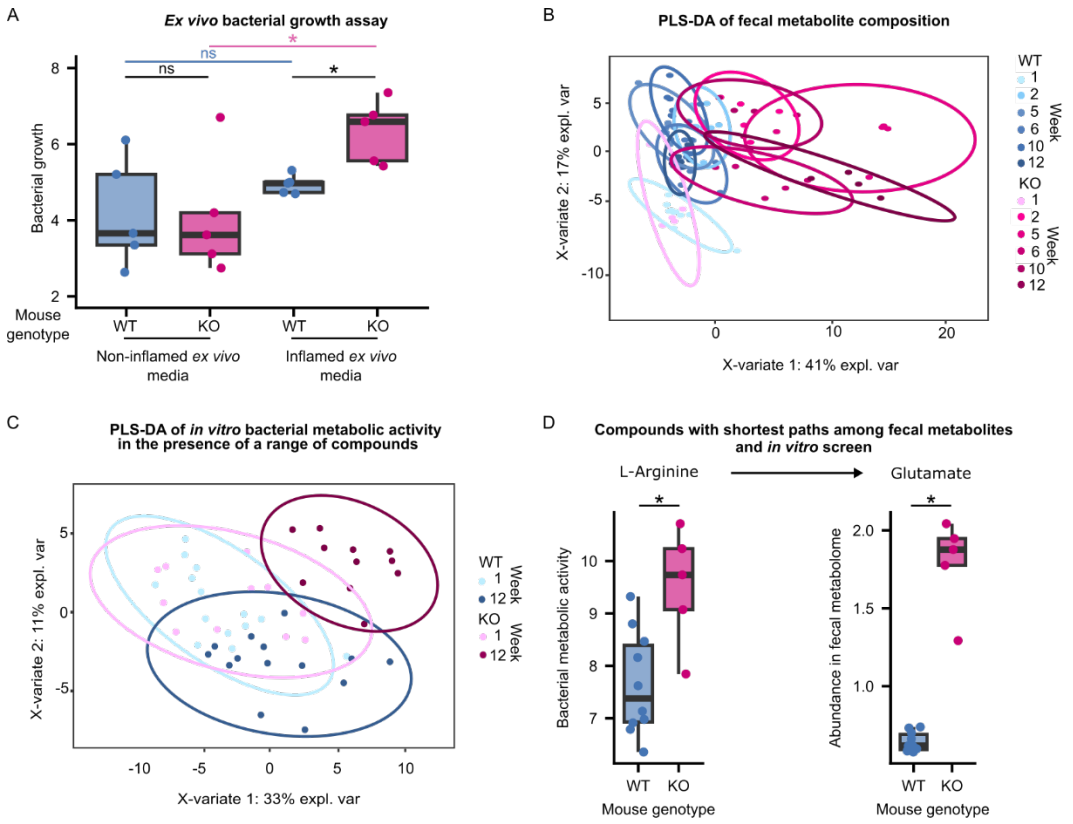

Figure 3. Phenotypic characterization of evolved *E. coli* and the inflammatory environment in which they were selected.

A Evolved populations from a subset of mice (n = 5 KO mice and n = 5 WT mice) were cultured in media derived from the cecal content collected from healthy (WT) and inflamed (KO) mice after sacrifice. The area under the curve (AUC) calculated from growth curves measured during the growth of evolved populations from each mouse in inflamed and healthy cecal contents is shown. Each dot represents the mean of three independent replicates. * $P < 0.05$ (Kruskal-Wallis H test); ns, not significant. **B** Partial least squares discriminant analysis (PLS-DA) of the fecal metabolite abundances at different time points during the evolution experiment. Differences were considered statistically significant at PERMANOVA $P < 0.05$ **C** Bacterial metabolism was measured *in- vitro* in a range of compounds. Measurements were performed on bacterial populations derived from fecal samples collected at weeks 1 and 12 of the *in-vivo* evolution experiments. Partial least squares discriminant analysis (PLS-DA) was performed on the area under the curves (AUCs) of the measured metabolic activity of the

735 evolved bacterial populations from all mice in the range of compounds. Differences were
736 considered statistically significant at PERMANOVA $P < 0.05$ **D** Compounds from the fecal
737 metabolome and the *in vitro* screen with the shortest path were inspected. One of the pairs
738 with the shortest path was glutamate-arginine. Glutamate was enriched in the fecal
739 metabolome of KO mice, whereas KO-adapted bacteria showed higher metabolic activity in
740 the presence of arginine. Each dot represents the abundance of the compound in the fecal
741 sample from a mouse (for glutamate) or the mean metabolic activity of the bacterial
742 population from a mouse in the presence of L-arginine from two independent measurements
743 (for arginine). * $P < 0.05$, (Kruskal-Wallis test at Benjamini-Hochberg-corrected), ns, not
744 significant.
745

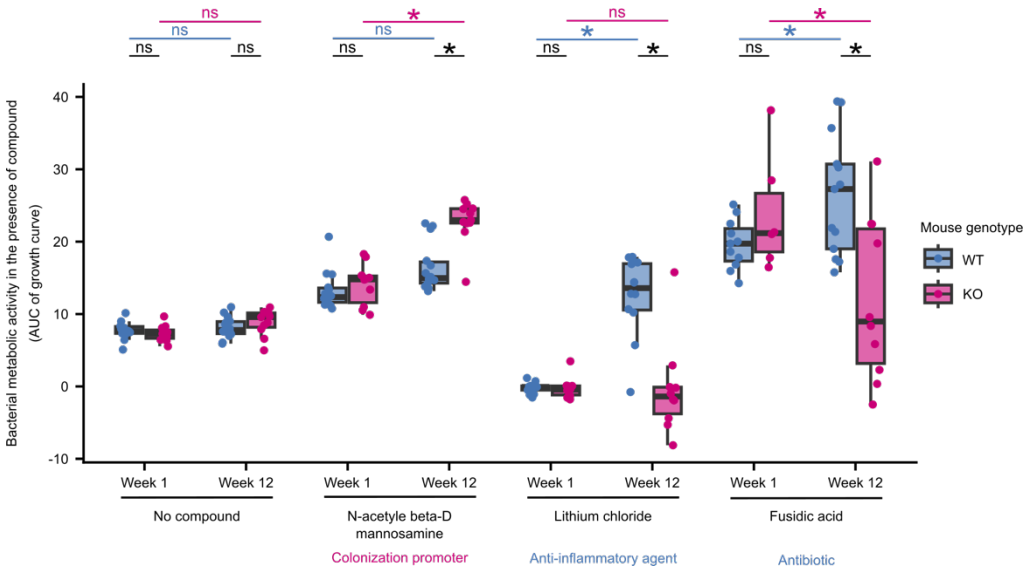

Figure 4. *E. coli* adapted to the inflamed gut show phenotypes with clinical relevance. Metabolic activity of bacteria isolated at weeks 1 and 12 of the evolution experiment in the presence of three selected compounds. Area under the curve was calculated from growth curves measured during the growth of evolved populations in the presence of each compound. Each dot represents the mean of two independent replicates of the metabolic activities of the *E. coli* population from a mouse measured in two independent experiments. *, $P < 0.05$ (Kruskal-Wallis test at Benjamini-Hochberg-corrected). The clinical relevance of the three compounds is indicated.

757 **References**

758

759 1. Ott, S. J. *et al.* Reduction in diversity of the colonic mucosa associated bacterial
760 microflora in patients with active inflammatory bowel disease. *Gut* **53**, 685–693 (2004).
761 2. Gevers, D. *et al.* The treatment-naïve microbiome in new-onset Crohn's disease. *Cell*
762 *Host Microbe* **15**, 382–392 (2014).
763 3. Rehman, A. *et al.* Geographical patterns of the standing and active human gut
764 microbiome in health and IBD. *Gut* **65**, 238–248 (2016).
765 4. Halfvarson, J. *et al.* Dynamics of the human gut microbiome in inflammatory bowel
766 disease. *Nat. Microbiol.* **2**, 17004 (2017).
767 5. Schirmer, M. *et al.* Dynamics of metatranscription in the inflammatory bowel disease
768 gut microbiome. *Nat. Microbiol.* **3**, 337–346 (2018).
769 6. Schirmer, M., Garner, A., Vlamakis, H. & Xavier, R. J. Microbial genes and pathways
770 in inflammatory bowel disease. *Nat. Rev. Microbiol.* **17**, 497–511 (2019).
771 7. Willing, B. P. *et al.* A pyrosequencing study in twins shows that gastrointestinal microbial
772 profiles vary with inflammatory bowel disease phenotypes. *Gastroenterology* **139**, 1844-
773 1854.e1 (2010).
774 8. Barreto, H. C. & Gordo, I. Intrahost evolution of the gut microbiota. *Nat. Rev. Microbiol.*
775 (2023) doi:10.1038/s41579-023-00890-6.
776 9. Giraud, A. *et al.* Costs and benefits of high mutation rates: adaptive evolution of bacteria
777 in the mouse gut. *Science* **291**, 2606–2608 (2001).
778 10. Paepe, M. D. *et al.* Trade-Off between Bile Resistance and Nutritional Competence
779 Drives Escherichia coli Diversification in the Mouse Gut. *PLOS Genet.* **7**, e1002107
780 (2011).

781 11. Barroso-Batista, J. *et al.* The First Steps of Adaptation of Escherichia coli to the Gut Are
782 Dominated by Soft Sweeps. *PLOS Genet.* **10**, e1004182 (2014).
783 12. Zhao, S. *et al.* Adaptive Evolution within Gut Microbiomes of Healthy People. *Cell Host*
784 *Microbe* **25**, 656-667.e8 (2019).
785 13. Elhenawy, W., Tsai, C. N. & Coombes, B. K. Host-Specific Adaptive Diversification of
786 Crohn's Disease-Associated Adherent-Invasive Escherichia coli. *Cell Host Microbe* **25**,
787 301-312.e5 (2019).
788 14. Barreto, H. C., Sousa, A. & Gordo, I. The Landscape of Adaptive Evolution of a Gut
789 Commensal Bacteria in Aging Mice. *Curr. Biol.* **30**, 1102-1109.e5 (2020).
790 15. Daniel, H. Diet and Gut Microbiome and the "Chicken or Egg" Problem. *Front. Nutr.* **8**,
791 (2022).
792 16. Garland, T., Downs, C. J. & Ives, A. R. Trade-Offs (and Constraints) in Organismal Biology.
793 *Physiol. Biochem. Zool. PBZ* **95**, 82–112 (2022).
794 17. Nesse, R. M., Ganten, D., Gregory, T. R. & Omenn, G. S. Evolutionary molecular
795 medicine. *J. Mol. Med. Berl. Ger.* **90**, 509–522 (2012).
796 18. Merker, M. *et al.* Evolutionary Approaches to Combat Antibiotic Resistance:
797 Opportunities and Challenges for Precision Medicine. *Front. Immunol.* **11**, (2020).
798 19. Roemhild, R. & Schulenburg, H. Evolutionary ecology meets the antibiotic crisis: Can we
799 control pathogen adaptation through sequential therapy? *Evol. Med. Public Health*
800 **2019**, 37–45 (2019).
801 20. Andersson, D. I. *et al.* Antibiotic resistance: turning evolutionary principles into clinical
802 reality. *FEMS Microbiol. Rev.* **44**, 171–188 (2020).
803 21. Melnikov, S. V. *et al.* Exploiting evolutionary trade-offs for posttreatment management
804 of drug-resistant populations. *Proc. Natl. Acad. Sci. U. S. A.* **117**, 17924–17931 (2020).

805 22. Hausser, J. *et al.* Tumor diversity and the trade-off between universal cancer tasks. *Nat.*
806 *Commun.* **10**, 5423 (2019).
807 23. Zhang, J., Cunningham, J. J., Brown, J. S. & Gatenby, R. A. Integrating evolutionary
808 dynamics into treatment of metastatic castrate-resistant prostate cancer. *Nat. Commun.*
809 **8**, 1816 (2017).
810 24. Jacqueline, C. *et al.* Cancer: A disease at the crossroads of trade-offs. *Evol. Appl.* **10**,
811 215–225 (2016).
812 25. Cunningham, J. J., Gatenby, R. A. & Brown, J. S. Evolutionary dynamics in cancer therapy.
813 *Mol. Pharm.* **8**, 2094–2100 (2011).
814 26. Kim, S. C., Tonkonogy, S. L., Karrasch, T., Jobin, C. & Sartor, R. B. Dual-association of
815 gnotobiotic IL-10-/- mice with 2 nonpathogenic commensal bacteria induces aggressive
816 pancolitis. *Inflamm. Bowel Dis.* **13**, 1457–1466 (2007).
817 27. Morgan, X. C. *et al.* Dysfunction of the intestinal microbiome in inflammatory bowel
818 disease and treatment. *Genome Biol.* **13**, R79 (2012).
819 28. Davenport, M. *et al.* Metabolic alterations to the mucosal microbiota in inflammatory
820 bowel disease. *Inflamm. Bowel Dis.* **20**, 723–731 (2014).
821 29. Brooun, A., Tomashek, J. J. & Lewis, K. Purification and Ligand Binding of EmrR, a
822 Regulator of a Multidrug Transporter. *J. Bacteriol.* **181**, 5131–5133 (1999).
823 30. Coll, J. L., Heyde, M. & Portalier, R. Expression of the *nmpC* gene of *Escherichia coli* K-12
824 is modulated by external pH. Identification of *cis* -acting regulatory sequences involved
825 in this regulation. *Mol. Microbiol.* **12**, 83–93 (1994).
826 31. Hirakawa, H. *et al.* AcrS/EnvR Represses Expression of the *acrAB* Multidrug Efflux Genes
827 in *Escherichia coli*. *J. Bacteriol.* **190**, 6276–6279 (2008).

828 32. Heinken, A. *et al.* Genome-scale metabolic reconstruction of 7,302 human
829 microorganisms for personalized medicine. *Nat. Biotechnol.* 1–12 (2023)
830 doi:10.1038/s41587-022-01628-0.
831 33. Huang, Y.-L., Chassard, C., Hausmann, M., von Itzstein, M. & Hennet, T. Sialic acid
832 catabolism drives intestinal inflammation and microbial dysbiosis in mice. *Nat. Commun.*
833 **6**, 8141 (2015).
834 34. Hofmann, C., Dunger, N., Schölmerich, J., Falk, W. & Obermeier, F. Glycogen synthase
835 kinase 3-β: A master regulator of toll-like receptor-mediated chronic intestinal
836 inflammation. *Inflamm. Bowel Dis.* **16**, 1850–1858 (2010).
837 35. Fernandes, P. Fusidic Acid: A Bacterial Elongation Factor Inhibitor for the Oral Treatment
838 of Acute and Chronic Staphylococcal Infections. *Cold Spring Harb. Perspect. Med.* **6**,
839 a025437 (2016).
840 36. Langholz, E., Brynskov, J., Bendtzen, K., Vilien, M. & Binder, V. Treatment of Crohn's
841 disease with fusidic acid: an antibiotic with immunosuppressive properties similar to
842 cyclosporin. *Aliment. Pharmacol. Ther.* **6**, 495–502 (2007).
843 37. Kilic, F. S., Erol, K., Batu, O., Yildirim, E. & Usluer, G. The effects of fusidic acid on the
844 inflammatory response in rats. *Pharmacol. Res.* **45**, 265–267 (2002).
845 38. Dapa, T., Ramiro, R. S., Pedro, M. F., Gordo, I. & Xavier, K. B. Diet leaves a genetic
846 signature in a keystone member of the gut microbiota. *Cell Host Microbe* **30**, 183-
847 199.e10 (2022).
848 39. Tawk, C. *et al.* Infection leaves a genetic and functional mark on the gut population of a
849 commensal bacterium. *Cell Host Microbe* **31**, 811-826.e6 (2023).

850 40. Sakamoto, A. *et al.* Three Members of Polyamine Modulon under Oxidative Stress
851 Conditions: Two Transcription Factors (SoxR and EmrR) and a Glutathione Synthetic
852 Enzyme (GshA). *PLoS ONE* **10**, e0124883 (2015).
853 41. Tian, T., Wang, Z. & Zhang, J. Pathomechanisms of Oxidative Stress in Inflammatory
854 Bowel Disease and Potential Antioxidant Therapies. *Oxid. Med. Cell. Longev.* **2017**,
855 4535194 (2017).
856 42. Carmel-Harel, O. & Storz, G. Roles of the Glutathione- and Thioredoxin-Dependent
857 Reduction Systems in the *Escherichia Coli* and *Saccharomyces Cerevisiae* Responses to
858 Oxidative Stress. *Annu. Rev. Microbiol.* **54**, 439–461 (2000).
859 43. Łyżeń, R., Gawron, G., Kadziński, L. & Banecki, B. GSH Protects the Escherichia coli Cells
860 from High Concentrations of Thymoquinone. *Molecules* **27**, 2546 (2022).
861 44. Pasternak, B. A. *et al.* Lipopolysaccharide exposure is linked to activation of the acute
862 phase response and growth failure in pediatric Crohn's disease and murine colitis.
863 *Inflamm. Bowel Dis.* **16**, 856–869 (2010).
864 45. Jagt, J. Z. *et al.* Fecal Amino Acid Analysis in Newly Diagnosed Pediatric Inflammatory
865 Bowel Disease: A Multicenter Case-Control Study. *Inflamm. Bowel Dis.* **28**, 755–763
866 (2022).
867 46. Stacy, A. *et al.* Infection trains the host for microbiota-enhanced resistance to
868 pathogens. *Cell* **184**, 615-627.e17 (2021).
869 47. Son, M., Ko, J. I., Kim, W. B., Kang, H. K. & Kim, B. K. Taurine can ameliorate
870 inflammatory bowel disease in rats. *Adv. Exp. Med. Biol.* **442**, 291–298 (1998).
871 48. Buret, A. G., Allain, T., Motta, J.-P. & Wallace, J. L. Effects of Hydrogen Sulfide on the
872 Microbiome: From Toxicity to Therapy. *Antioxid. Redox Signal.* **36**, 211–219 (2022).

873 49. Maeda, T. *et al.* Role of polyamines derived from arginine in differentiation and
874 proliferation of human blood cells. *Biol. Pharm. Bull.* **29**, 234–239 (2006).
875 50. Revilla-Nuin, B. *et al.* Transport of N-acetyl-D-mannosamine and N-acetyl-D-glucosamine
876 in Escherichia coli K1: effect on capsular polysialic acid production. *FEBS Lett.* **511**, 97–
877 101 (2002).
878 51. Freland, L. & Beaulieu, J.-M. Inhibition of GSK3 by lithium, from single molecules to
879 signaling networks. *Front. Mol. Neurosci.* **5**, 14 (2012).
880 52. Inaba, K. *et al.* Lithium toxicity and Na+(Li+)/H+ antiporter in Escherichia coli. *Biol.*
881 *Pharm. Bull.* **17**, 395–398 (1994).
882 53. Chen, C. C., Tsuchiya, T., Yamane, Y., Wood, J. M. & Wilson, T. H. Na+ (Li+)-proline
883 cotransport in Escherichia coli. *J. Membr. Biol.* **84**, 157–164 (1985).
884 54. Gatenby, R. A. & Brown, J. S. Integrating evolutionary dynamics into cancer therapy.
885 *Nat. Rev. Clin. Oncol.* **17**, 675–686 (2020).
886 55. Ezraty, B. & Barras, F. The 'liaisons dangereuses' between iron and antibiotics. *FEMS*
887 *Microbiol. Rev.* **40**, 418–435 (2016).
888 56. Cai, Z., Wang, S. & Li, J. Treatment of Inflammatory Bowel Disease: A Comprehensive
889 Review. *Front. Med.* **8**, 765474 (2021).
890 57. Öhman, L. *et al.* Fecal microbiota dynamics during disease activity and remission in
891 newly diagnosed and established ulcerative colitis. *Sci. Rep.* **11**, 8641 (2021).
892 58. Kim, S. C. *et al.* Variable phenotypes of enterocolitis in interleukin 10-deficient mice
893 monoassociated with two different commensal bacteria. *Gastroenterology* **128**, 891–
894 906 (2005).
895 59. Moolenbeek, C. & Ruitenberg, E. J. The 'Swiss roll': a simple technique for histological
896 studies of the rodent intestine. *Lab. Anim.* **15**, 57–59 (1981).

897 60. Adolph, T. E. *et al.* Paneth cells as a site of origin for intestinal inflammation. *Nature* **503**,
898 272–276 (2013).
899 61. Martin, M. Cutadapt removes adapter sequences from high-throughput sequencing
900 reads. *EMBnet.journal* **17**, 10 (2011).
901 62. KneadData – The Huttenhower Lab. https://huttenhower.sph.harvard.edu/kneaddata/.
902 63. Bolger, A. M., Lohse, M. & Usadel, B. Trimmomatic: a flexible trimmer for Illumina
903 sequence data. *Bioinformatics* **30**, 2114–2120 (2014).
904 64. Deatherage, D. E. & Barrick, J. E. Identification of Mutations in Laboratory-Evolved
905 Microbes from Next-Generation Sequencing Data Using breseq. in *Engineering and*
906 *Analyzing Multicellular Systems* (eds. Sun, L. & Shou, W.) vol. 1151 165–188 (Springer
907 New York, 2014).
908 65. Love, M. I., Huber, W. & Anders, S. Moderated estimation of fold change and dispersion
909 for RNA-seq data with DESeq2. *Genome Biol.* **15**, 550 (2014).
910 66. Kitamoto, S. *et al.* Dietary L-serine confers a competitive fitness advantage to
911 Enterobacteriaceae in the inflamed gut. *Nat. Microbiol.* **5**, 116–125 (2020).
912 67. Haslauer, K. E., Schmitt-Kopplin, P. & Heinzmann, S. S. Data Processing Optimization in
913 Untargeted Metabolomics of Urine Using Voigt Lineshape Model Non-Linear Regression
914 Analysis. *Metabolites* **11**, 285 (2021).
915 68. Dieterle, F., Ross, A., Schlotterbeck, G. & Senn, H. Probabilistic Quotient Normalization
916 as Robust Method to Account for Dilution of Complex Biological Mixtures. Application in
917 1H NMR Metabonomics. *Anal. Chem.* **78**, 4281–4290 (2006).
918 69. Heinzmann, S. S., Waldenberger, M., Peters, A. & Schmitt-Kopplin, P. Cluster Analysis
919 Statistical Spectroscopy for the Identification of Metabolites in 1H NMR Metabolomics.
920 *Metabolites* **12**, 992 (2022).

70. Csárdi, G. & Nepusz, T. The igraph software package for complex network research. in (2006).
71. R: A Language and Environment for Statistical Computing | BibSonomy. https://www.bibsonomy.org/bibtex/7469ffee3b07f9167cf47e7555041ee7.
72. Faust, K., Croes, D. & van Helden, J. Metabolic pathfinding using RPAIR annotation. *J. Mol. Biol.* **388**, 390–414 (2009).
73. Ebrahim, A., Lerman, J. A., Palsson, B. O. & Hyduke, D. R. COBRApy: COnstraints-Based Reconstruction and Analysis for Python. *BMC Syst. Biol.* **7**, 74 (2013).
74. Anderson, M. J. A new method for non-parametric multivariate analysis of variance. *Austral Ecol.* **26**, 32–46 (2001).
75. Bray, J. R. & Curtis, J. T. An Ordination of the Upland Forest Communities of Southern Wisconsin. *Ecol. Monogr.* **27**, 325–349 (1957).
76. Rohart, F., Gautier, B., Singh, A. & Cao, K.-A. L. mixOmics: an R package for 'omics feature selection and multiple data integration. 108597 Preprint at https://doi.org/10.1101/108597 (2017).
77. Signorell, A. *et al.* DescTools: Tools for Descriptive Statistics. (2023).